Prediction of Three-Phase Capillary Pressure using a Network Model Anchored to Two-Phase Data

Elisabeth Iren Dale[1,2], Marinus I. J. van Dijke[3] and Arne Skauge[1]

[1]*Centre for Integrated Petroleum Research - University of Bergen*

[2]*StatoilHydro*

[3]*Heriot-Watt University*

Corresponding author: Elisabeth Iren Dale, StatoilHydro, Postbox 7190, 5020 Bergen, Norway elid@statoilhydro.com

Abstract

Three-phase capillary pressure is difficult to measure experimentally and therefore has to be estimated by other methods. In this work a network model was applied to generate a consistent set of two-phase and three-phase capillary pressure curves.

Experimental data for two-phase, gas-oil and oil-water, capillary pressure from a North Sea reservoir was used in this study. The network model was anchored to the measured two-phase data, and three-phase capillary pressure was constructed.

The gas-oil and mercury capillary pressure anchors the pore structure parameters, while water-oil capillary pressure anchors the wettability parameters in the network model. The three-phase capillary pressure is predicted by using the pore structure and wettability found for the two-phase cases as input.

The network model quantifies the difference between two-phase and three-phase capillary pressure. In the cases studied the difference between two-phase and three-phase capillary pressure is significant.

Keywords: Capillary pressure, three-phase, network model, mixed-wet.

1. Introduction

Capillary pressure is an important parameter when describing reservoir behaviour. Capillary pressure had a large effect on history match of relative permeability curves (Dale and Skauge, 2007). There is an increased need to model three-phase performance, e.g. because of the use of water-alternating-gas-injection (WAG).

Two-phase capillary pressure is relatively easy to measure in the laboratory, but three-phase capillary pressure is seldom available from experiments. Kalaydjian's paper (1992) is one of the few reported cases of measurements of three-phase capillary pressure.

One common way to model three-phase capillary pressure is by using weighted averages between the two-phase, gas-oil and oil-water, curves (Killough, 1976). This model is illustrated in figure 1, where the dashed lines are the two-phase capillary pressure curves, and the solid lines represent the three-phase capillary pressure curves. The purpose of this work was to find out if this is a good approximation.

Network models can be used to predict three-phase behavior. The concept of using a network of pores to model flow in porous media was first described by Fatt (1956, part I-III). The concept was not further investigated before the 1980s (Koplik, 1982; Wilkinson and Willemsen, 1983), when percolation theory (Stauffer and Aharony, 1992) was incorporated in network models. The network models can be used to explain and predict many pore scale phenomena. Blunt (2001) has given a summary of the major advances in network modeling.

Several network models able to model three-phase behavior have been developed (Fenwick and Blunt, 1998; Mani and Mohanty, 1998; Øren et al., 1998; van Dijke and Sorbie, 2002; Valvatne and Blunt, 2004; Piri and Blunt, 2005b). A few examples of estimation of three-phase capillary pressure exists (Fenwick and Blunt, 1998; Mani and Mohanty, 1998; Suicmez et al., 2006).

A network simulator (van Dijke *et al.*, 2001; van Dijke and Sorbie, 2002) developed at the Heriot-Watt University was used in this work. This network model can be used to match two-phase data and predict three-phase data. The input parameters found from the two-phase match is used as input data for the three-phase simulations.

Svirsky *et al.* (2004) obtained reasonable predictions of three-phase relative permeability with this network model. Both two- and three-phase relative permeability experimental data, for a

water-wet Berea sandstone, was available. The model was anchored to the two-phase data and the predicted three-phase relative permeability was compared to the measured three-phase data.

van Dijke *et al.* (2006) used two-phase data from a mixed-wet North Sea reservoir. The measured two-phase data was used to anchor the network model. Relative permeabilities and capillary pressures for several three-phase gas displacements, starting at different initial water saturations, were predicted.

In this paper predictions of three-phase capillary pressure for a different North Sea reservoir is presented. The first part of the paper is a description of the main features of the network model. Then, a summary of the available experimental data is given. A detailed description of the method for matching the two-phase data, the anchoring process, is provided. Three-phase capillary pressure is predicted from this anchored model, and is compared to the two-phase capillary pressure.

2. Network simulator

A network simulator able to handle three-phase flow in porous media with heterogeneous wettability was constructed at the Heriot-Watt University (van Dijke *et al.*, 2001; van Dijke and Sorbie, 2002). The simulator is based on capillary driven invasion percolation, the flow is capillary dominated.

To simulate experimental behaviour the "3R approach" is used (McDougall *et al.*, 2001). The network model consists of a three-dimensional network of pores with radius r. The distribution of r is taken from a given minimum and maximum radius together with the pore size distribution. In this case a simple power law function was used for the pore size distribution, given as

$$f(r) \propto r^n . \qquad (1)$$

The shape of the gas oil curve is strongly dependent on this distribution. The power law exponent was one of the main tuning parameters in the matching process.

The capillary pressure, the volume and conductance are all functions of the radius

$$P_c \propto \frac{1}{r}, \tag{2}$$

$$V(r) \propto r^{\nu} \quad \text{and} \tag{3}$$

$$g(r) \propto r^{\lambda}. \tag{4}$$

The expression for Pc is consistent with the Young-Laplace equation. The volume exponent is normally in the range of 0 to 2, and the conductance exponent is normally in the range of 1 to 4. The volume exponent is equal to 2 for a cylinder and the conductivity exponent is equal to 4 in Poiseuilles law.

The connectivity of the network is also important to include. The z factor quantifies the average number of exits and entrances from the pores in the network. The number can be between 1 and 6, but values less than 2.5 are rarely used.

The wettability is described by contact angles between oil and water, given as $\cos\theta_{ow}$. It is also possible to use an ageing option in the network model. Then you can use different wettabilities before and after ageing of the core. Ageing options has also been implemented in other network models (Øren et al., 1998; Piri and Blunt, 2002; Valvatne and Blunt, 2004).

In our case a primary drainage down to the irreducible water saturation was performed at water-wet conditions. Then the core was aged and after ageing the wettability was mixed-wet large, large pores oil-wet. In the case of mixed-wet large, the input value is also the transition radius between oil-wet and water-wet pores, $r(\text{wet})$.

The degree of films and layers also has to be described. This is done by giving threshold values for the contact angles, where layers are formed above these values. When layers are present it is possible for a fluid to escape through a pore as a film or layer even though the fluid is not the main occupant of the pore. A high level of films and layers will result in a low level of trapping.

A boundary condition with constant outlet pressure is used. Capillary pressures are taken as the pressure of the invading phase minus that of the outlet phase involved in a displacement.

See discussion section for more details on the boundary condition and calculation of capillary pressures.

3. Experimental data

Capillary pressure data from a North Sea reservoir was used in this study. Two-phase, gas-oil and oil-water, capillary pressures were measured on core plugs with oil and irreducible water saturation using a centrifuge. The Skjæveland *et al.* (2000) correlation was used to represent the measured data, see figures 3 and 4.

Mercury data was available, but for a core with slightly different properties than the cores used in the capillary pressure measurements. No certain data of the pore size distribution could be found from mercury data.

Wettability was measured from the same core as the oil-water capillary pressure. The wettability was considered to be mixed-wet. The Amott index was lower than the USBM index which indicates a mixed-wet large state; big pores oil-wet and small pores water-wet.

A flooding case with a composite core was also available. The composite core had similar properties as the core where capillary pressure and wettability data were measured. The interfacial tensions between the fluids were not measured. The gas-oil and oil-water capillary pressure curves were scaled to match the irreducible water saturation and endpoint saturations from the flooding experiment of initial gas injection and the initial water injection, respectively.

4. Match with network simulator, anchoring the model

The two-phase capillary pressure data was matched using the network simulator. Mercury data can often be used to estimate the minimum and maximum pore radius and the pore size distribution, because in the case of mercury-air the interfacial tension and wettability are known parameters. The gas-oil capillary pressure can also be used to anchor the pore properties as it is less dependent on wettability than the oil-water capillary pressure. The oil-water capillary pressure is used to determine the wettability parameters.

This general procedure for matching capillary pressure is however not always precise. Often the gas-oil capillary pressure is somewhat affected by the wettability. It is therefore important to do some iterations of the match of the gas-oil and oil-water capillary pressures after the

main tendencies for the wettability and pore properties are determined. A summary of the workflow is shown in figure 2.

Run parameters: The core was initially filled with water when starting the network simulation. The first flood is a primary drainage down to irreducible water saturation. This is the starting position for both the gas-oil and oil-water capillary pressure match. The core is at the starting point oil-filled with approximately 30% irreducible water and 70% oil. When matching the gas-oil capillary pressure gas is injected, and when matching water-oil capillary pressure water is injected.

Fluid properties: The interfacial tension values were not measured experimentally and common values for these parameters had to be chosen. Common values for these parameters are

$\sigma_{go} \approx 0$ to ~ 20 mN/m (always the lowest),

$\sigma_{ow} \sim$ 20 to ~ 40 mN/m and

$\sigma_{gw} \sim$ 40 to ~ 60 mN/m (always the largest).

The values chosen were σ_{go} equal to 15 mN/m, σ_{ow} equal to 35 mN/m and σ_{gw} equal to 45 mN/m.

The spreading coefficient is given as

$$C_{s,o} = \sigma_{gw} - \sigma_{ow} - \sigma_{go} \tag{5}$$

and has to be less than or equal to zero. It is often assumed that σ_{gw} adjusts at equilibrium to give $C_{s,o} \leq 0$. When the spreading coefficient is equal to zero the oil spreads as a layer between the gas and water. If the coefficient is negative the oil is not spreading. The values were chosen to ensure a non-spreading oil phase ($C_{s,o} = 45 - 35 - 15 = -5$).

Pore properties: The pore geometry is given by the minimum pore radius, the maximum pore radius and the pore size distribution. The $r(\max)$ and $r(\min)$ value can often be determined directly from modelling the mercury data, as they are connected to the displacement capillary pressure and the maximum capillary pressure, respectively. In this case the mercury data was from a core with different properties than the one used for the capillary pressure

measurements and the mercury intrusion did not go to 100% saturation. The estimated $r(\min)$ and $r(\max)$ from the mercury data therefore had to be adjusted when running the gas-oil case. The connection between $r(\max)$ and the displacement pressure, and $r(\min)$ and the maximum pressure is also strong in the gas-oil case.

Another tuning parameter was the coordination number, z, which quantifies pore connectivity. The minimum and maximum possible coordination number was found by matching the irreducible water saturation in the primary drainage. When assuming oil films z was equal to 1.9, and when assuming no oil films z was equal to 4.5. The practical lower limit was however approximately 3.5. When using a coordination number lower than 3.5 the residual oil saturation was too high after water flooding. It was possible to get a good match for the capillary pressure with both the minimum and maximum coordination number. The coordination number equal to 3.5 was chosen as the best match. This coordination number gave the result which was closest to the shape of the capillary pressure curves from the experimental data.

A low value for the volume exponent was chosen to achieve a high enough irreducible water saturation after primary drainage.

The gas-oil capillary pressure was now matched satisfactorily and the next step was to match the oil-water capillary pressure. The same parameters used as input to the gas-oil case were now used in the oil-water case. The wettability parameters were tuned to get a match of the oil-water capillary pressure.

Wettability parameters: The aging option was enabled. The wettability before aging was chosen to be water-wet. The contact angle was tuned until the correct irreducible water saturation was achieved. A high threshold value for the parameter "Min. gas-water cos(angle) for water film around gas/oil" ensured that the irreducible water was not produced during the later injection periods.

After the primary drainage and ageing the wettability was assumed to develop into mixed-wet large, large pores oil-wet. The wettability is described by the angle between the oil and water phase, $\cos\theta_{ow}$. Distributed contact angles were used. The shape of the oil-water capillary pressure curve is affected by the cosine of the contact angle for the water-filled, oil-filled water-wet and oil-filled oil-wet pores. Low oil-filled oil-wet values (weakly oil-wet) will e.g.

reproduce low negative capillary pressure values, as is seen in the experimental data. The "oil-filled oil-wet" pores was therefore set to be weakly oil-wet.

The fraction of the pores called "oil-filled oil-wet" pores represent the large oil-filled pores. The part of the pores called "oil-filled water-wet pores" does not necessarily have to be water-wet. This fraction just represents the small oil-filled pores. Parts of the so-called "water-wet" oil-filled pores can actually be the most oil-wet in the system. The smallest oil-filled pores are the last pores to be entered by water and therefore represent the area close to the negative asymptote on the oil-water capillary pressure curve. In order to get a high negative value close to the asymptote some of these pores need to be oil-wet.

Tuning of the parameter "Max. oil-water cos(angle) for oil film around water" gave the correct maximum water saturation during water flooding. The parameter "Max. gas-oil cos(angle) for oil film around gas" provided the correct maximum gas saturation during the gas flooding. The place where the oil-water capillary pressure crosses the x-axis depends strongly on the radius of change between oil-wet and water-wet pores, $r(wet)$.

After matching the oil-water capillary pressure all the parameters, including those for wettability, were used as input to the gas-oil case. The gas-oil capillary pressure curve was slightly different. Wettability had a small effect also on the gas-oil capillary pressure in this case. An iteration process for fine-tuning the pore properties and wettability parameters in order to match both curves with the same parameters was necessary.

The match of the gas-oil capillary pressure is shown in figures 3, and the match of the oil-water capillary pressure is shown in figures 4. The grey line represents the measured data, and the black line is the match from the network model. All the parameters used in the match are summarized in table 1.

The irregularities of the curves occur because the network size is limited. A model with an infinite number of pores would give a smooth curve and the most accurate results, but would of course take for ever to run. A compromise between accuracy and run time must be found. A network with size 15 x 15 x 15 pores was chosen. The method used for matching was "trial-and-error" and the runtime for the 15 x 15 x 15 model was a bit long for this method. The model has to be small when the "trial-and-error" method is used because it takes a lot of iterations to reach a satisfactory match. A network model with 10 x 10 x 10 pores was therefore used to run sensitivities. After a satisfactory match was reached with this small

network the parameters found was tested in the 15 x 15 x 15 network, and the resulting capillary pressure curves were approximately the same. This suggests that the 10 x 10 x 10 network actually was big enough to capture the fundamental nature of the porous medium.

One problem with matching capillary pressure by using a network model is that it is very time consuming when many parameters are unknown. A more automatic optimization method is therefore under development. Another issue is if there is only one combination of parameters which produces a match of the experimental data. It seems to be possible to get similar matches with different input-values. There might not be a unique solution to this problem. In this case two capillary pressure curves are matched with the same set of parameters, and that might constrain the problem enough to make it possible to find a unique solution.

5. Prediction of three-phase capillary pressure

After anchoring to the two-phase capillary pressure an attempt was made to predict the three-phase capillary pressure curves.

The input parameters established for the two-phase match were used. Two three-phase flooding cases after primary drainage to irreducible water saturation were run. One flooding sequence started with initial water injection and secondary gas injection, W1G2. The other sequence started with gas injection and was followed by water injection, G1W2. The matched two-phase gas-oil capillary pressure from initial gas injection, G1, was then compared to the predicted three-phase gas-oil capillary pressure from secondary gas injection, G2. The same was performed for oil-water capillary pressure, where the matched initial water injection, W1, was compared to the predicted secondary water injection process, W2.

The results for the gas-oil two- and three-phase capillary pressures are shown in figure 5. The gas-water capillary pressures for gas injection are shown in figure 6.

The predicted three-phase gas-oil capillary pressure is significantly higher than the matched two-phase gas-oil capillary pressure. The same was observed by van Dijke *et al.* (2006) for gas injection into a core with high initial water saturation. The three-phase gas-oil capillary pressure from secondary gas injection, G2, is higher than for two-phase, G1. The maximum gas saturation for G2 is lower indicating more trapped water, but the trapped oil saturations are about the same; see the saturation path for W1G2 in figure 9. The gas-water capillary pressure, seen in figure 6, is much higher for the two-phase case than for three-phase flow.

Figure 7 shows the results for the oil-water capillary pressure. The gas-water capillary pressures for water injection are shown in figure 8.

The predicted three-phase oil-water capillary pressure for W2 is also significantly different from the two-phase capillary pressure. As seen in figure 7 this capillary pressure is larger and entirely negative. The W2 process has a lower maximum water saturation than the W1 process, indicating that trapped gas is present; see the saturation path for G1W2 in figure 9. On the other hand, residual oil saturation is about 5% lower after W2. The gas-water capillary pressure has large negative values for the two-phase case, see figure 8. However, this curve is an artefact, as during W1 no gas is present.

The predicted three-phase gas-oil and oil-water capillary pressures are significantly different from the two-phase capillary pressures. The magnitude of the capillary pressure curves is different and the endpoint saturation values are different.

6. Synthetic water-wet case

A simple water-wet case was also tested. This case had the same pore properties as the field case and the same wettability parameters before ageing as used in the mixed-wet case, but water-wet after ageing. The cosine to the contact angle used after ageing is 0.95. The parameters for films and layers are the same as for the mixed-wet case. The general trends of the results from the water-wet case were the same as for the more complex mixed-wet case.

The gas-oil capillary entry pressure for three-phase was slightly higher than for two-phase, see figure 10. The gas-water capillary pressure is high for two-phase and low for three-phase (not shown). The saturation path for the W1G2 case can be seen in figure 12.

The three-phase oil-water capillary pressure crosses the x-axis and becomes negative, even though the two-phase case does not cross the saturation axis at all, see figure 11. Notice that one would always expect a positive oil-water capillary pressure for a two-phase system. The saturation path for G1W2 can be seen in figure 12. The residual oil is high because only a small amount of the pores have films and layers.

7. Discussion

The behaviour of tree-phase capillary pressures is complex. Kalaydjian (1992) measured three-phase capillary pressures on an outcrop water-wet core and on unconsolidated material. He found that the three-phase capillary pressures depended on all three saturation values. He also found indications that the capillary pressure was larger in absolute value for three-phase than for two-phase flow.

The network model also predicts larger three-phase than two-phase capillary pressures. The gas-oil capillary pressure curves have larger positive values and the oil-water curves have larger negative values than their two-phase counterparts. The three-phase capillary pressure curves seem to be on the outside of the two-phase capillary pressure loop, instead of inside the loop as in Killough's model (1976).

Accessibility may be one of the main reasons why the three-phase capillary pressure is higher than the two-phase capillary pressures. In three-phase flow the alternating injection of gas and water can produce snap-off and bypass, which may lead to discontinuous phases. Consequently, the invading phase does not have access to as many pores as would be the case in two-phase flow. This will affect the pressure in the system. The invading phase could be forced to take a different path with higher entry pressures and also double or multiple displacements may be the result.

One effect of reduced accessibility is that no direct displacement of oil is possible. Double or multiple displacement chains may then be necessary to create a connected displacement path from inlet to outlet. When displacement chains with multiple interfaces occur, the capillary pressure will depend on the forces at all interfaces. (Øren and Pinczewski, 1995). For example, during gas injection gas may not be able to displace oil directly with

$$P_{C,go}^{3-ph} = P_{C,go}^{effective} = P_{C,go}\,. \tag{6}$$

Instead, the less favourable double displacement may occur, where gas displaces water, which in turn displaces oil. For this displacement the effective capillary pressure between gas at the inlet and oil at the outlet depends on the capillary pressure between gas and water and on the capillary pressure between water and oil, at the respective interfaces,

$$P_{C,go}^{3-ph} = P_{C,go}^{effective} = P_{C,gw} + P_{C,wo}\,. \tag{7}$$

The effective capillary pressure of the double displacement may then be higher than that for the direct displacement.

For further details regarding the capillary pressure for double displacements see the paper by Øren and Pinczewski (1995), and for multiple displacements see the paper by van Dijke and Sorbie (2002).

The choice of boundary conditions is important for the magnitude of the three-phase capillary pressures. In this paper constant boundary conditions have been used, which means that during each flood the pressures at the outlet are kept constant and only the invading phase pressure is increased (at the inlet).The "historic maximum" of invading phase pressure is used, i.e. this pressure is monotonically increasing, even during spontaneous displacements. When changing the invading phase (new flood), pressures at the outlet are updated using the final capillary pressures of the preceding flood (van Dijke and Sorbie, 2002; Mani and Mohanty, 1998). Global capillary pressures follow from the pressure of the invading phase minus the pressure of the phase at the outlet that is involved in the displacement (chain). For a gas flood, a displacement with an oil cluster at the outlet directly provides the gas-oil capillary pressure as

$$P_{C,go}^{3-ph} = P_{C,go}^{effective} \tag{8}$$

Then, the gas-water capillary pressure is given by

$$P_{C,gw}^{3-ph} = P_{C,go}^{effective} + P_{C,ow}(outlet) \tag{9}$$

where $P_{C,ow}(outlet)$ is the constant oil-water pressure difference taken from the preceding flood, which is also considered as the global oil-water capillary pressure.

In contrast, so-called varying outlet boundary conditions could also be used (van Dijke and Sorbie, 2002 ; Piri and Blunt, 2005; Suicmez et al., 2007). These conditions allow the outlet pressure difference and the associated global capillary pressure to vary with the reconnection

of disconnected phases. For example, during a gas flood, a disconnected oil cluster may reconnect to the outlet through a multiple displacement chain, in which case the outlet oil pressure is adjusted to the pressure of the reconnecting oil cluster.

The above can explain a number of trends in the capillary pressure curves of both the mixed-wet case (Figures 5, 6, 7 and 8) and the water-wet case (Figures 10 and 11). Comparing the saturation paths for the gas floods G1 and G2 for the mixed-wet case, shown in Figure 9, we find that during G1 gas almost exclusively displaces oil, as oil is well connected. Hence, the (global) gas-oil capillary pressure presented in Figure 5, is almost identical to the two-phase gas-oil capillary pressure of Figure 3. On the contrary, during G2 gas displaces mainly water. Hence, the (global) gas-water capillary pressure presented in Figure 6 is almost identical to a two-phase gas-water curve (not shown). Similar to equation (9), the corresponding gas-oil capillary pressure curve (Figure 5) incorporates the constant oil-water outlet pressure difference as $P_{C,go}^{3-ph} = P_{C,gw}^{effective} - P_{C,ow}(outlet)$. According to the constant boundary conditions, $P_{C,ow}(outlet)$ is taken as the value of the oil-water capillary pressure at the end of the preceding water flood W1, which is presented in Figure 7. As mentioned earlier, parts of the so-called “water-wet” oil-filled pores are actually the most oil-wet in the system. Due to lack of accessibility a fraction of these pores have been invaded by water, yielding the large negative $P_{C,ow}$ value at the end of W1, i.e. the $P_{C,ow}(outlet)$ during G2, which suggests the large gas-oil “entry” pressure for G2 in Figure 5. Moreover, comparison of the gas-oil capillary pressure curves for G1 and G2 in Figure 5, shows that for G2 $P_{C,go}^{3-ph}$ values have been achieved that are much larger than those resulting from simple two-phase gas-oil displacements. This is caused by the lack of accessibility and the choice of boundary conditions.

At the start of G2, oil is mostly disconnected, hence gas has to displace some water from the system first, with $P_{C,go}^{3-ph} = P_{C,gw}^{effective} - P_{C,ow}(outlet)$, where $P_{C,gw}^{effective}$ could reflect double or multiple displacement chains involving disconnected oil clusters. Following these initial displacements, a number of displacement chains occur, through which some oil is removed from the system, see figure 9 for S_g between 0.3 and 0.4. For these displacements the effective gas-oil capillary pressures $P_{C,go}^{3-ph} = P_{C,go}^{effective}$ are similar to the global $P_{C,gw}^{3-ph}$. The steep

increase at the end of the curves for G2 in Figures 5 and 6 relate to gas displacing water from smaller and smaller pores.

Similarly, the W2 curve reflects many displacements, through which gas is displaced from the system, see figure 9. In this case $P_{C,ow}^{3-ph} = P_{C,gw}^{effective} - P_{C,go}(outlet)$, with $P_{C,go}(outlet)$ identical to the end value of G1. The gas-water capillary pressure values, $P_{C,gw}^{effective}$, are small, as water displaces gas from the larger pores (see also Figure 8).

The trends for the capillary pressure curves corresponding to water-wet case can be explained similarly. Most strikingly, the oil-water capillary pressure curve for W2 in Figure 11 is negative. In an entirely two-phase water-wet system, this would never have been possible, and can only occur in a three-phase context.

In summary, the higher 3-phase Pc can have several explanations. Lower accessibility for three-phase flow might increase the capillary pressure, and the choice of boundary conditions is also important.

The most important question is if the boundary conditions used make sense on core and field scale. A core flooding experiment is usually done with a constant pressure at the outlet of the core. The assumption of constant boundary conditions in the network might be suitable for this case. On field scale the picture is more complicated. The assumption might however not be valid in the three-phase zone. In the three-phase zone the oil will, in many cases, be discontinuous and the oil pressure will then vary with the pressure in the surrounding phases. The varying boundary condition in the network model could therefore be preferred in that situation.

To predict three-phase capillary pressures you have to use the network model and anchor it for your specific case. Then, for each saturation history, different three-phase capillary curves arise. Therefore, it is probably not easy or maybe not even possible to generate a universal correlation for this three-phase behaviour.

8. Conclusions

- The network model is sufficiently flexible to reproduce experimental gas-oil and oil-water capillary pressure data adequately. The match of the gas-oil capillary pressure was very good, and the match of the oil-water capillary pressure was reasonably good.
- The predicted three-phase capillary pressures are significantly different from the two-phase capillary pressures. A synthetic water-wet case produces similar results as the complex mixed-wet case.
- The endpoint saturation values were in some cases different for three-phase capillary pressure and two-phase capillary pressure because of trapping.
- The absolute values of the capillary pressures were higher for three-phase than for two-phase. The gas-oil capillary pressure for three-phase had a higher positive value, and the three-phase oil-water capillary pressure had a higher negative value.
- The higher capillary pressure for three-phase flow might be explained by lower accessibility and the boundary conditions. The chosen boundary condition seems reasonable for core floods.
- A weighted average between the two-phase curves can not describe these predicted three-phase curves.
- It is very time consuming to match the two-phase capillary pressure and it is not certain that it is possible to find a unique solution. More measured data or a software for optimization is needed.

Nomenclature

$C_{s,o}$	spreading coefficient, oil
f	function
g	conductivity
n	power law exponent
P_c	capillary pressure
$P_{C,go}$	two-phase gas-oil capillary pressure
$P_{C,go}^{effective}$	effective gas-oil capillary pressure
$P_{C,go}^{3-ph}$	three-phase gas-oil capillary pressure
$P_{C,go}(outlet)$	gas-oil capillary pressure at the outlet

$P_{C,gw}$	gas-water capillary pressure
$P_{C,ow}$	oil-water capillary pressure
$P_{C,ow}^{3-ph}$	three-phase oil-water capillary pressure
$P_{C,ow}(outlet)$	oil-water capillary pressure at the outlet
r	radius
$r(\text{wet})$	radius for change of wettability
V	volume
z	coordination number
θ_{ow}	contact angle between oil and water
λ	conductivity exponent
ν	volume exponent
σ_{go}	interfacial tension between gas and oil
σ_{ow}	interfacial tension between oil and water
σ_{gw}	interfacial tension between gas and water

References

Blunt, M. J.: “Flow in porous media — pore-network models and multiphase flow”, Curr. Opin. Colloid Interface Sci, pp. 197–207, 2001.

Dale, E. I., and Skauge, A.: “Features Concerning Capillary Pressure and the Effect on Two-Phase and Three-Phase Flow”, paper for the 14th European Symposium on Improved Oil Recovery, Cairo, Egypt, 22. – 24. April 2007.

Eclipse simulation software manual 2006.1, Technical description.

Fatt, I.: “The network model of porous media I. Capillary pressure characteristics.”, Trans AIME, 207, pp. 144–159, 1956.

Fatt, I.: “The network model of porous media II. Dynamic properties of a single size tube network.”, Trans AIME, 207, pp. 160–163, 1956.

Fatt, I.: “The network model of porous media III. Dynamic properties of networks with tube radius distribution.”, Trans AIME, 207, pp. 164–181, 1956.

Fenwick, D. H., and Blunt, M. J.: “Network modelling of three-phase flow in porous media”, SPEJ 3(1), pp 86-97, 1998.

Kalaydjian, F. J-M.: “Performance and Analysis of Three-Phase Capillary Pressure Curves for Drainage and Imbibition in Porous Media,” paper SPE 24878 presented at the 1992 SPE Annual Technical Conference and Exhibition, Washington, DC, 4–7 October, 1992.

Killough, J. E.: “Reservoir Simulation with History-dependent Saturation Functions”, Trans. AIME 261, pp. 37–48, 1976.

Koplik, J.: “Creeping flow in two-dimensional networks”, J. Fluid Mech., 119, pp. 219–247, 1982.

Mani, V., and Mohanty, K. K.: “Pore-level network modelling of three-phase capillary pressure and relative permeability curves, SPEJ 3, pp. 337-353, 1998.

McDougall, S. R., Cruickshank, J. and Sorbie, K. S.: “Anchoring Methodologies for Pore-Scale Network Models: Application to Relative Permeability and Capillary Pressure Prediction”, proceedings of the 2001 International Symposium of the Society of Core Analysts, Edinburgh, 2001.

Piri, M., and Blunt M. J.: “Three-dimensional mixed-wet pore-scale network modeling of two- and three-phase flow in porous media. II. Results.”, Phys. Rev. E. 71, 026302, 2005.

Skjæveland, S. M., Siqveland, L. M., Kjosavik, A., Hammervold Thomas, W. L. and Virnovsky, G. A.: “Capillary Pressure Correlation for Mixed-Wet Reservoirs”, SPE Reservoir Evaluation & Engineering 3, pp. 60-67, February 2000.

Stauffer D., and Aharony, A.: “Introduction to Percolation Theory”, 2nd Edition, Taylor & Francis, London, 1992.

Suicmez, V. S., Piri, M., and Blunt, M. J.: “Pore-scale Simulation of Water Alternate Gas Injection”, Transport in Porous Media Vol. 66, No. 3, pp. 259-286, February 2007.

Svirsky, D. S., van Dijke, M. I. J., and Sorbie, K. S.: “Prediction of Three-Phase Relative Permeabilities Using a Pore-Scale Network Model Anchored to Two-Phase Data”, SPE 89992, proceedings of SPE ATCE, Houston, TX, 2004.

Valvatne, P. H., and Blunt, M. J.: Predictive pore-scale modelling of two-phase flow in mixed-wet media”, W07406, Water Resour. Res., 40(7), 2004.

van Dijke, M. I. J., McDougall, S. R., and Sorbie, K. S.: “Three-Phase Capillary Pressure and Relative Permeability Relationships in Mixed-Wet Systems”, Transport in Porous Media 44, pp. 1–32, 2001.

van Dijke, M. I. J. and Sorbie, K. S.: “Pore-Scale Network Model for Three-Phase Flow in Mixed-Wet Porous Media”, Phys. Rev. E., 66, 046302, 2002.

van Dijke, M. I. J., Sorbie, K. S. and de Mik, F.: ”Network model prediction of three-phase relative permeabilities for a mixed-wet reservoir based on anchoring to two-phase data”, proceedings Symposium on Reservoir Wettability, Bergen, Norway, September 2006.

Wilkinson, D., and Willemsen, J. F.: “Invasion percolation: a new form of percolation theory”, J. Phys. A., 16, pp. 3365–3370, 1983.

Øren, P. E., and Pinczewski, W. V: “Fluid Distribution and Pore-Scale Displacement Mechanisms in Drainage Dominated Three-Phase Flow”, Transport in Porous Media, 20, pp. 105–133, 1995.

Øren, P.E., Bakke, S., and Arntzen, O. J.: “Extending Predictive Capabilities to Network Models”, SPEJ, 3(4), pp. 324-336, December 1998.

Table 1: Summary of input data in the network model

Pore properties	
r(min)	1e-07
r(max)	1.5e-005
n (Power law exponent)	-0.6
z (Coordination number)	3.5
ν (Volume exponent)	0.1
Wettability parameters	
Before ageing:	
Max. cos (contact angle)	1
Min. cos (contact angle)	0.75
After ageing:	
Wetting model	Mixed-Wet Large
Max. water-filled cos (contact angle)	1
Min. water-filled cos (contact angle)	0.8
r(wet) (minimum oil-wet/maximum water-wet radius)	7e-006
Max. oil-filled "water-wet" cos (contact angle)	0.5
Min. oil-filled "water-wet" cos (contact angle)	-0.96
Max. oil-filled oil-wet cos (contact angle)	0
Min. oil-filled oil-wet cos (contact angle)	-0.2
Films and layers: threshold values:	
Max. oil-water cos(angle) for oil film around water	-0.02
Min. gas-oil cos(angle) for oil film or spreading layer around gas	0.8392
Min. oil-water cos(angle) for water film around oil	0.98
Min. gas-water cos(angle) for water film around gas	1

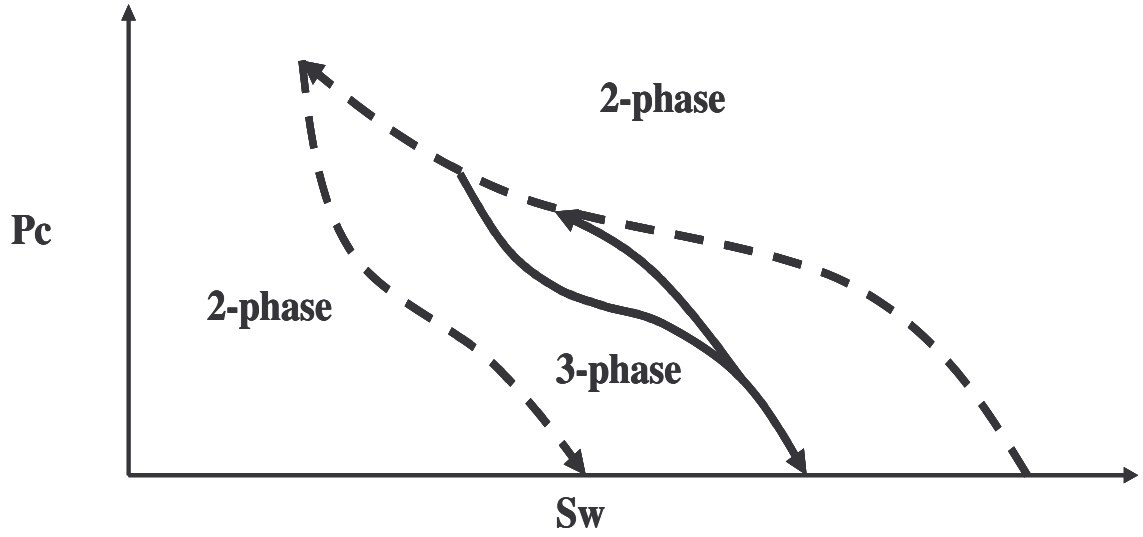

Fig. 1: Three-phase capillary pressure as a weighted average of the two-phase curves (Adapted from Eclipse technical description, 2006.1).

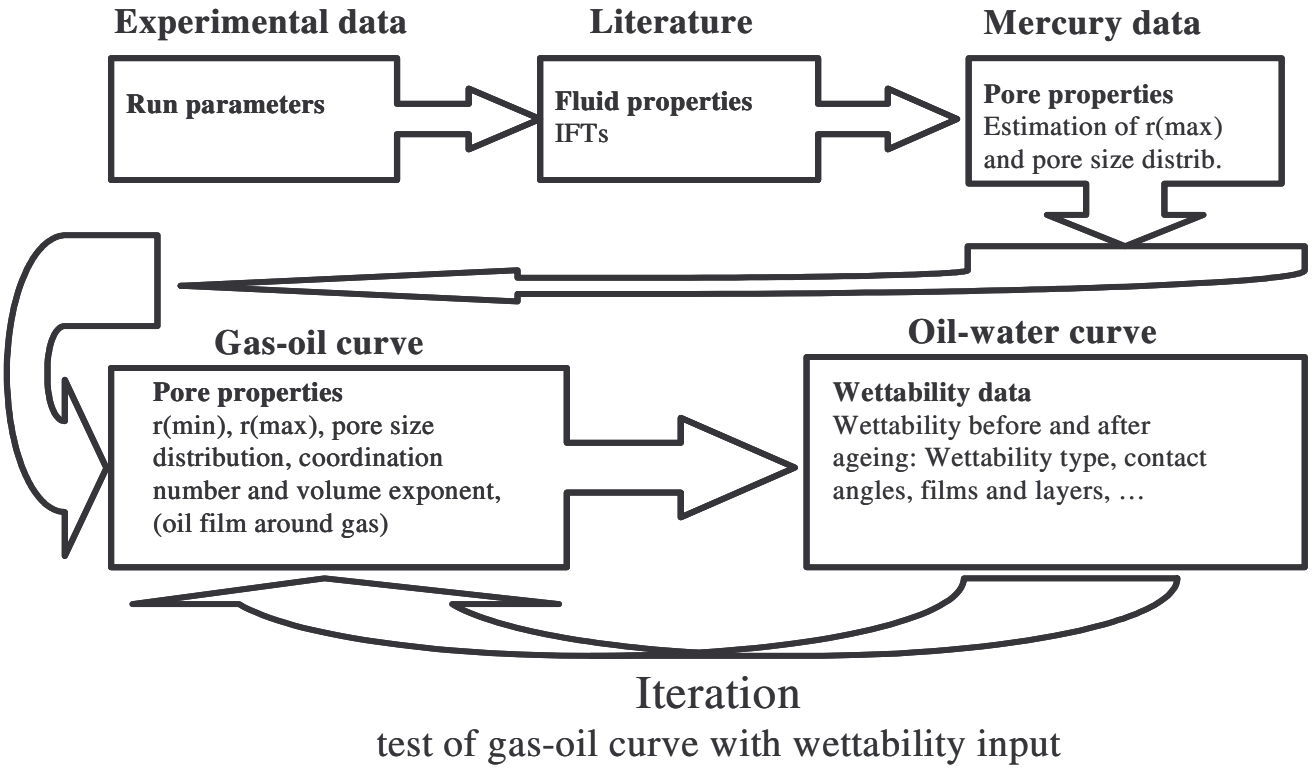

Fig. 2: Workflow for match of capillary pressure with the network model.

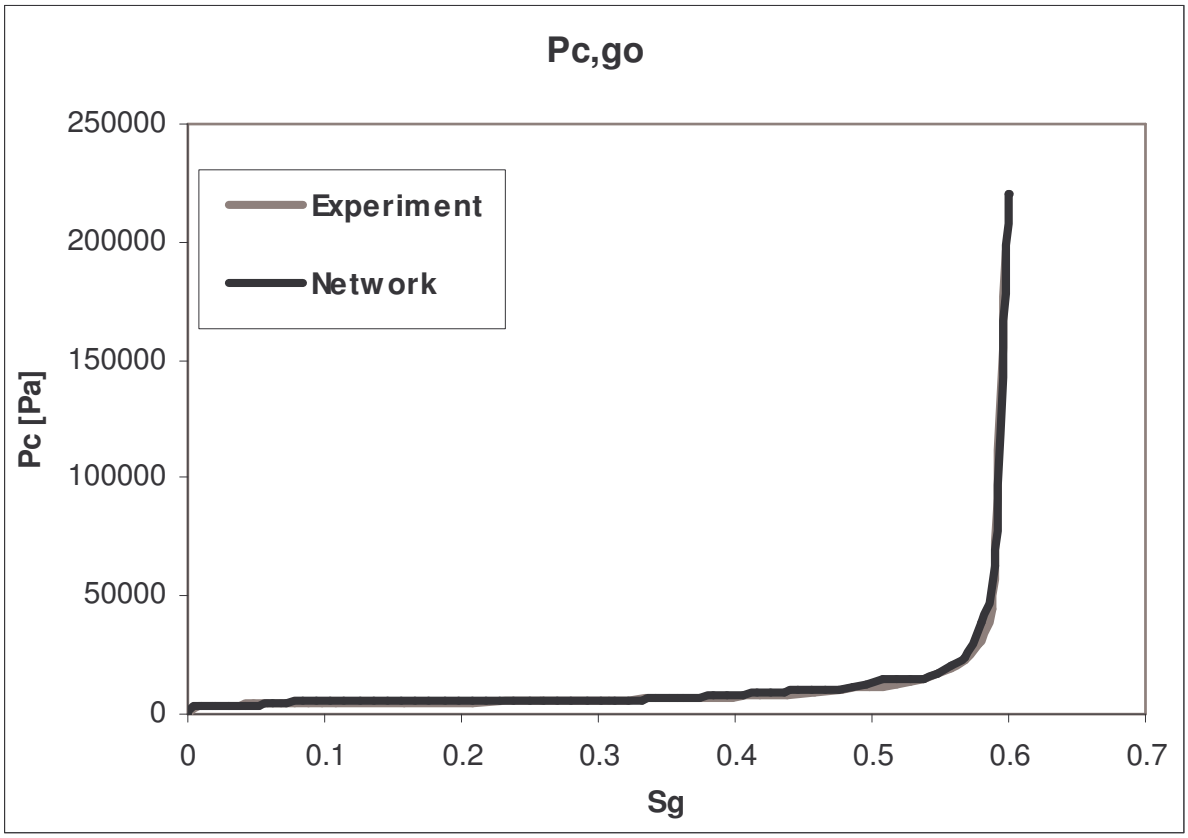

Fig. 3: Match of capillary pressure for the gas-oil process.

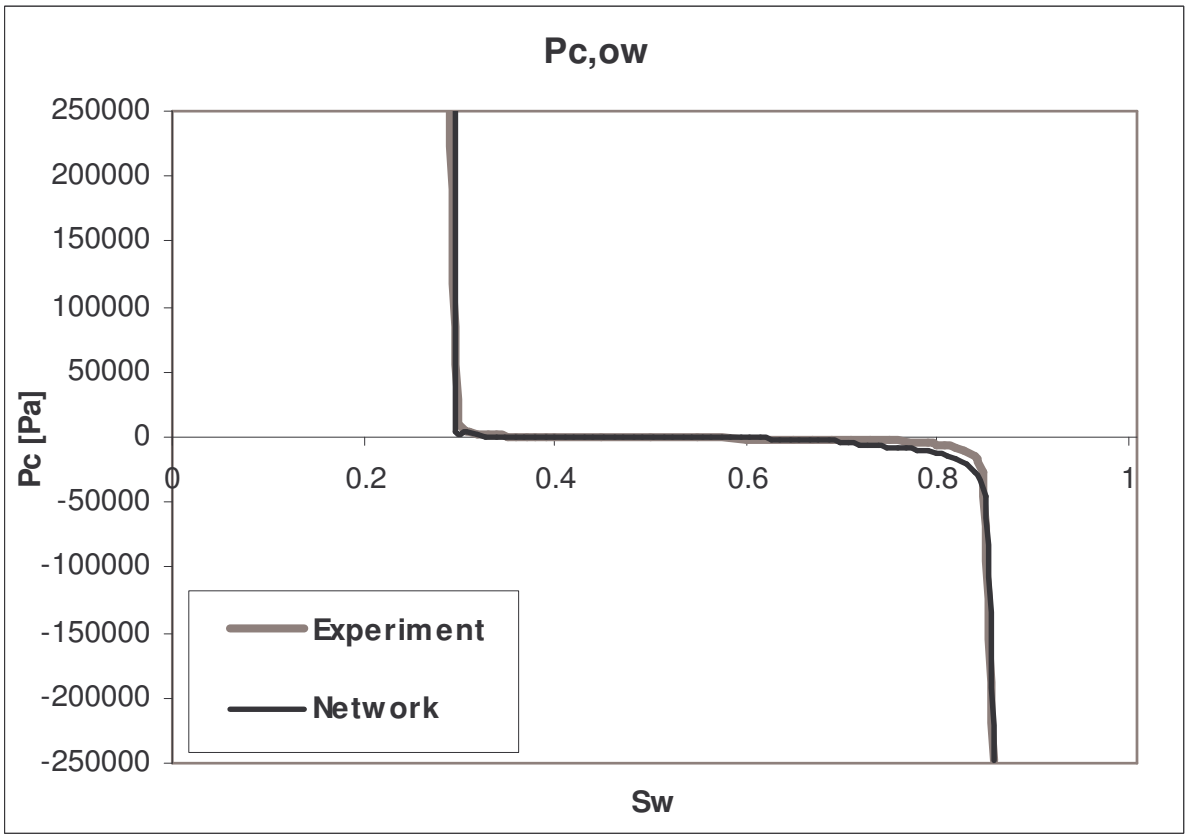

Fig. 4: Match of capillary pressure for the oil-water process.

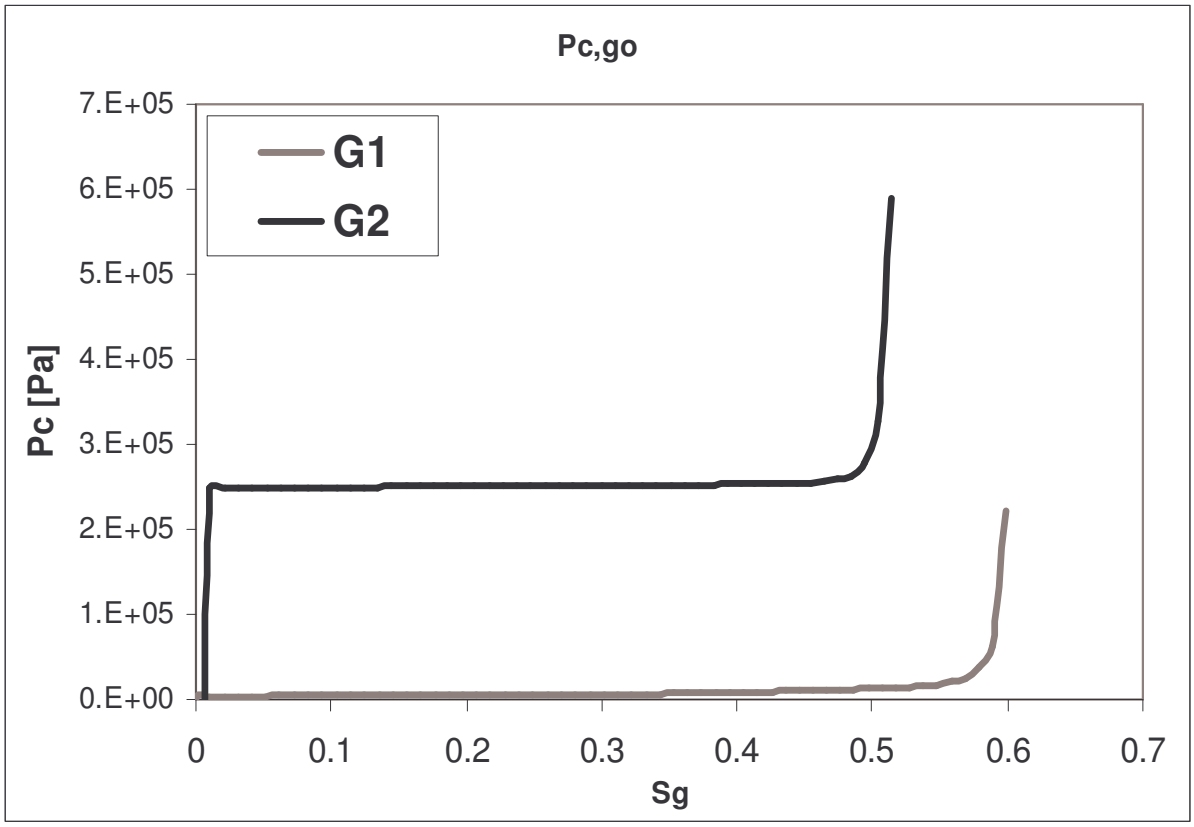

Fig. 5: Prediction of three-phase capillary pressure compared to two-phase capillary pressure for gas-oil.

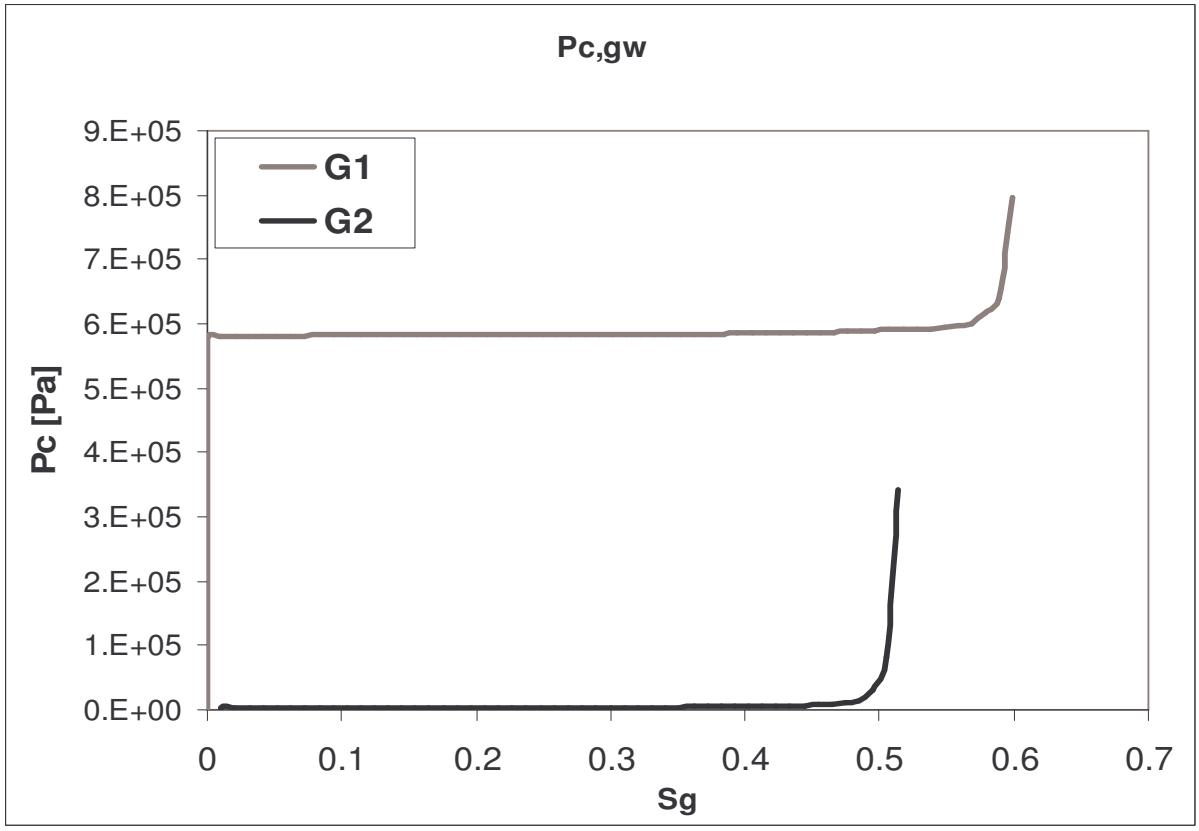

Fig. 6: Three-phase capillary pressure compared to two-phase capillary pressure for gas-water, when injecting gas.

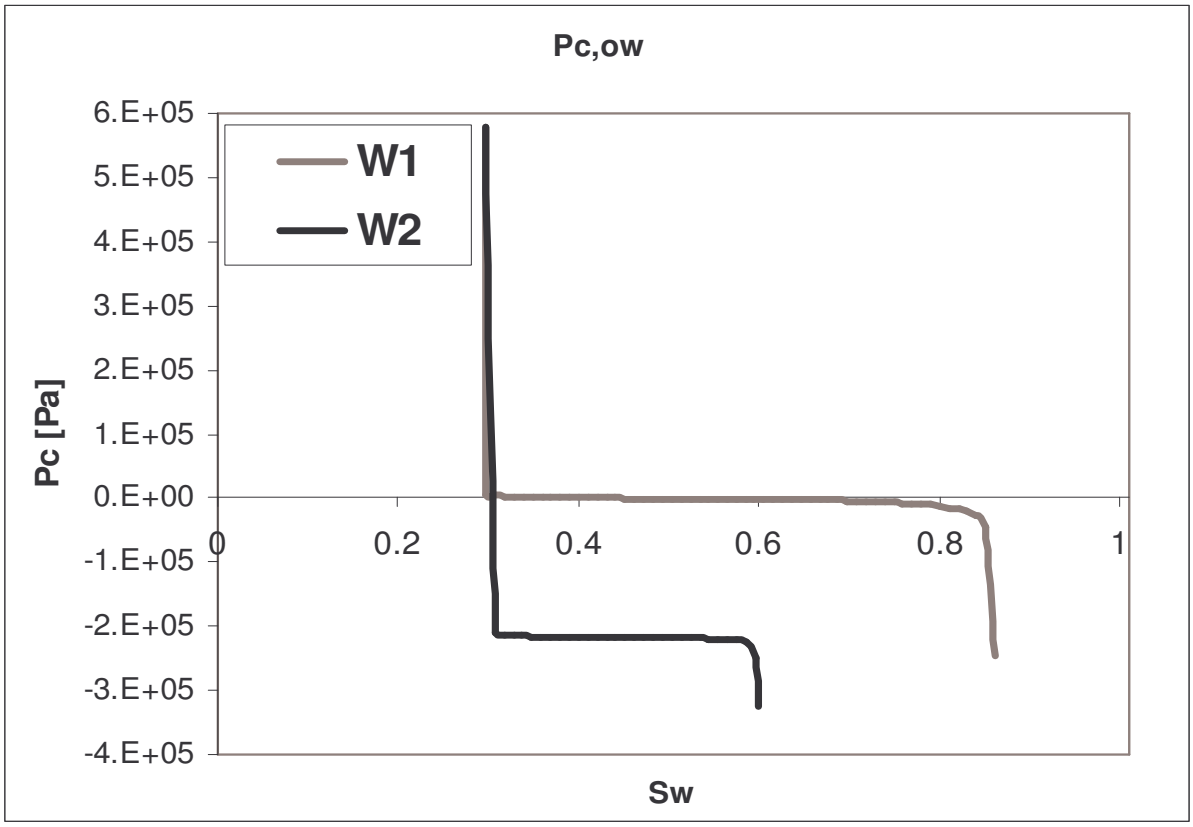

Fig. 7: Prediction of three-phase capillary pressure compared to two-phase capillary pressure for oil-water.

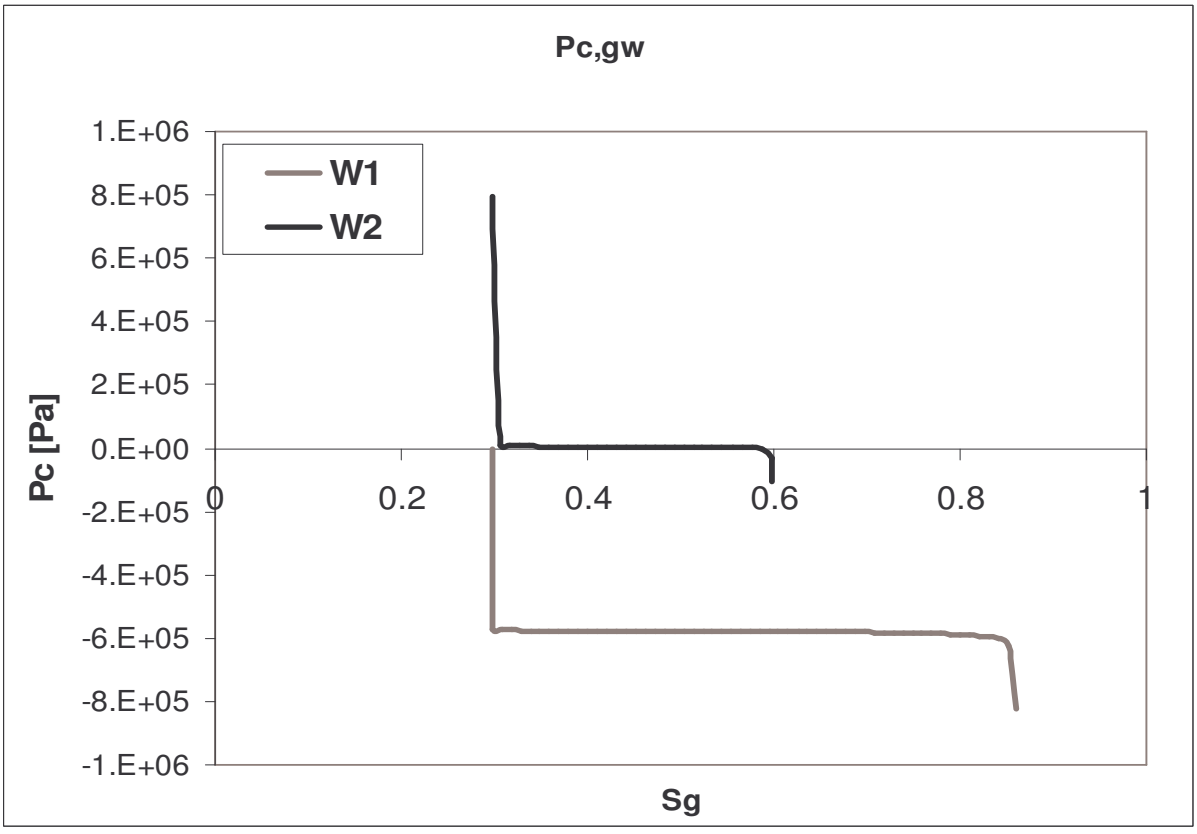

Fig. 8: Three-phase capillary pressure compared to two-phase capillary pressure for gas-water, when injecting water.

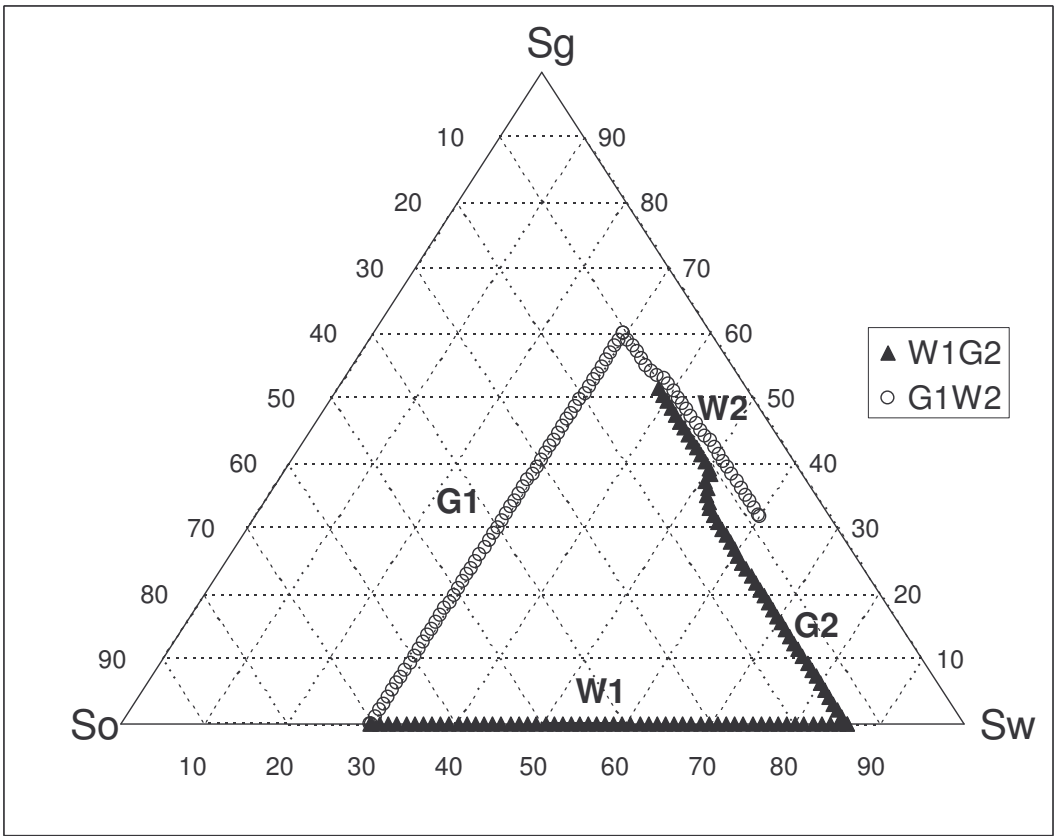

Fig. 9: Saturation paths for W1G2 and G1W2.

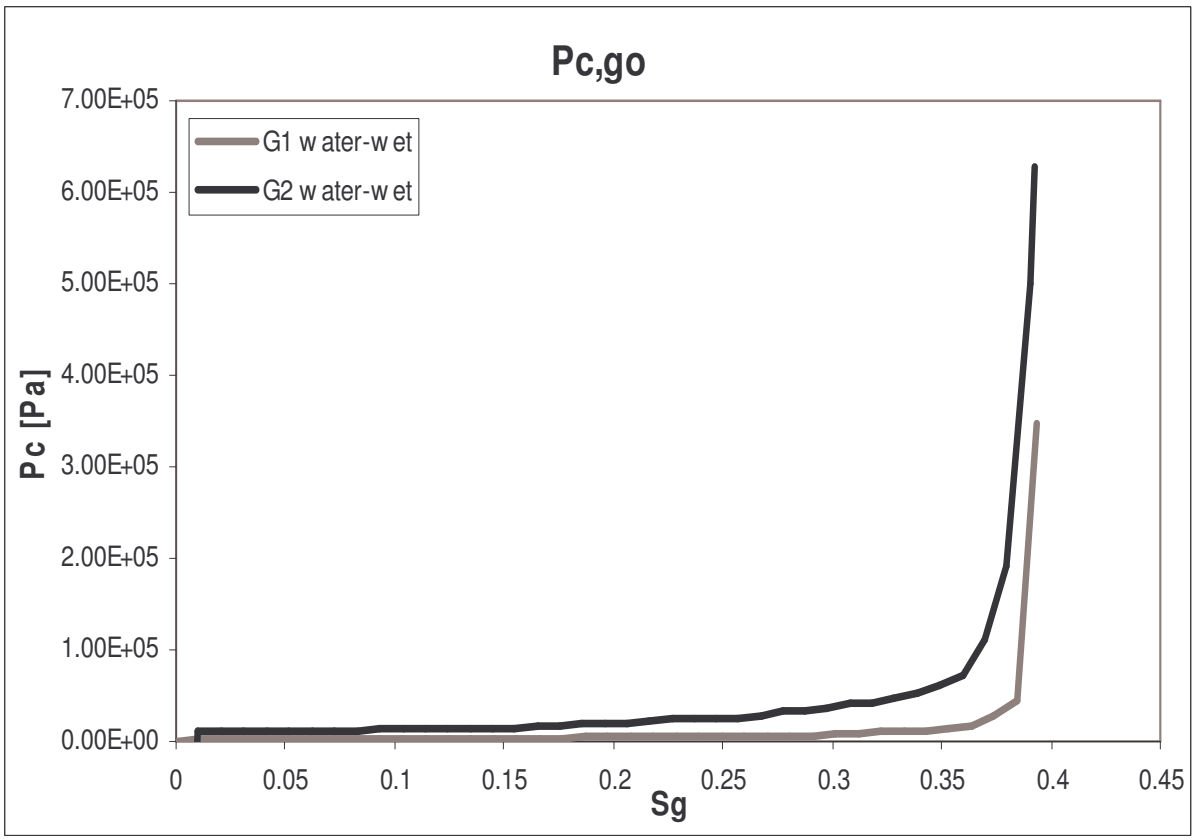

Fig. 10: Prediction of three-phase capillary pressure compared to two-phase capillary pressure for gas-oil, water-wet case.

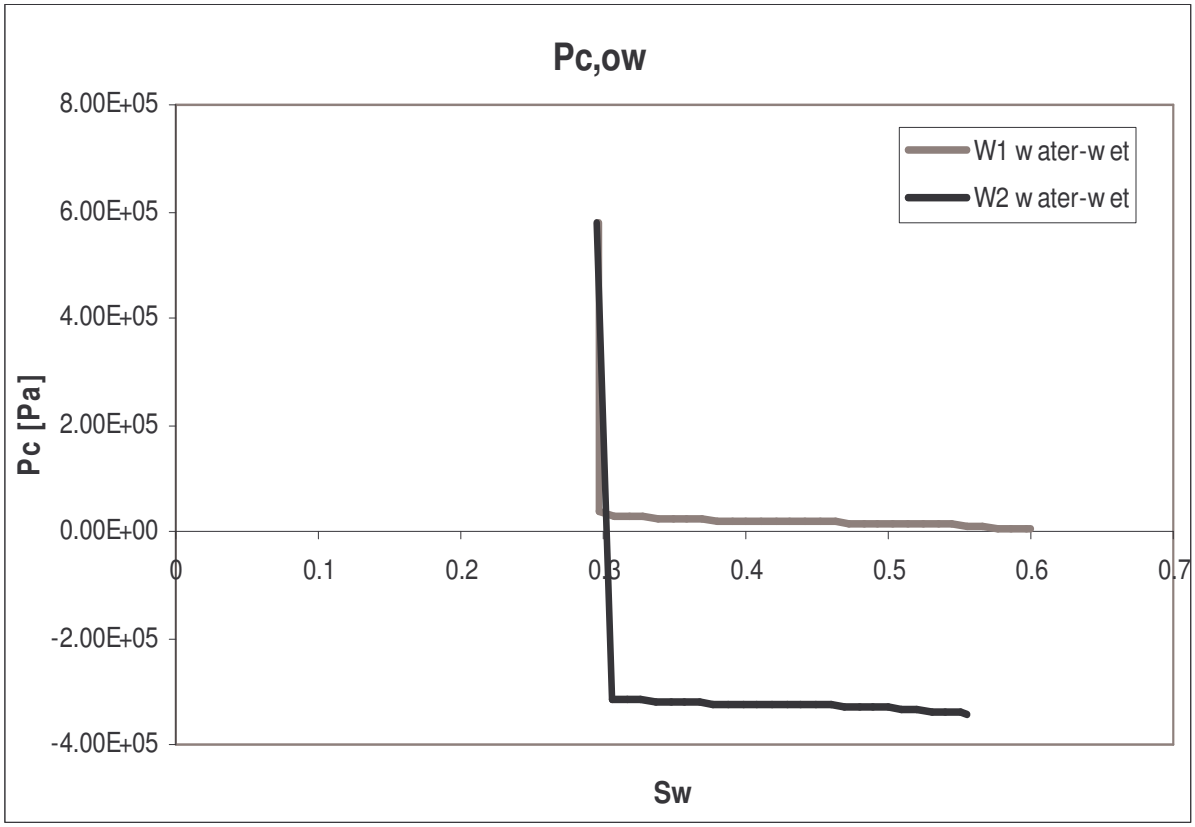

Fig. 11: Prediction of three-phase capillary pressure compared to two-phase capillary pressure for oil-water, water-wet case.

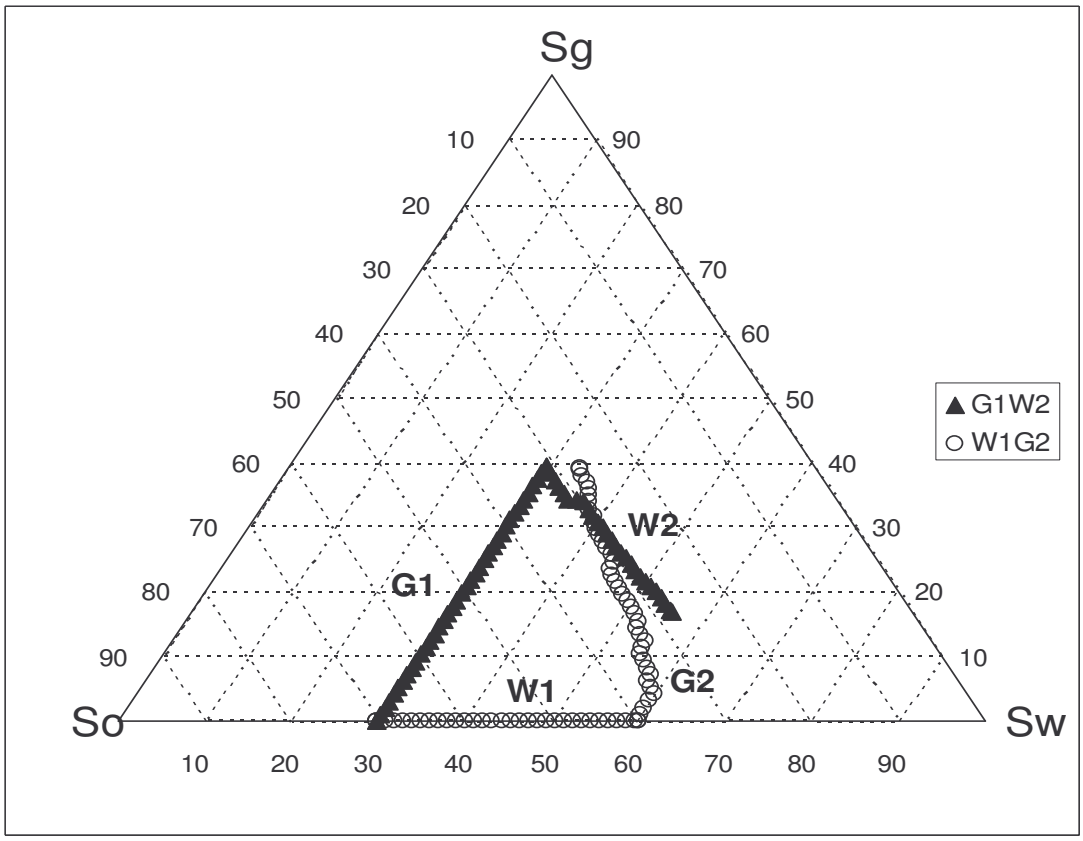

Fig. 12: Saturation path for the initial gas secondary water injection process, G1W2, water-wet case.